Applied Physics Letters

RESEARCH ARTICLE | JULY 24 2023

Correlation of metal-to-insulator transition and strain state of VO_2 thin films on TiO_2 (110) substrates

Hao Lu; Lei Li; Zhiwu Tang; Maji Xu; Yonghui Zheng; Martin Becker; Yinmei Lu; Mingkai Li; Pai Li; Zaoli Zhang; Peter J. Klar; Yunbin He

Appl. Phys. Lett. 123, 042103 (2023)
https://doi.org/10.1063/5.0152809

Articles You May Be Interested In

$RuVO_2$ alloy epitaxial films: Lowered insulator–metal transition temperature and retained modulation capacity

Appl. Phys. Lett. (May 2020)

Achieving p-type conductivity in wide-bandgap SnO_2 by a two-step process

Appl. Phys. Lett. (March 2021)

High performance solar-blind UV detector based on $Hf_{0.38}Sn_{0.62}O_2$ epitaxial film

Appl. Phys. Lett. (June 2020)

27 September 2024 08:12:58

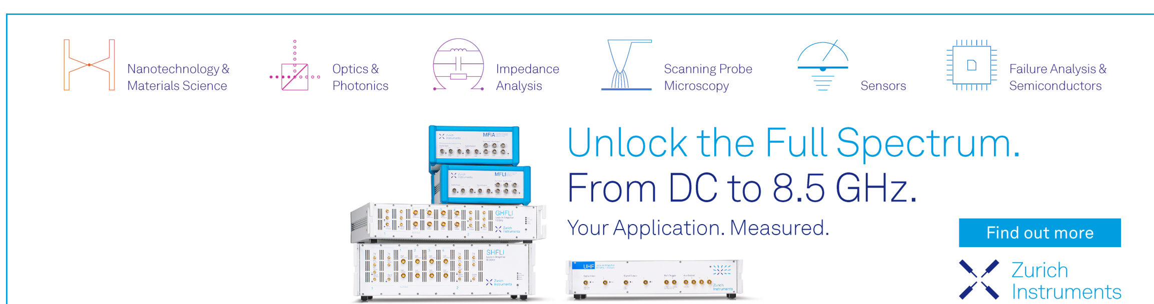

Correlation of metal-to-insulator transition and strain state of VO_2 thin films on TiO_2 (110) substrates

Cite as: Appl. Phys. Lett. **123**, 042103 (2023); doi: 10.1063/5.0152809
Submitted: 1 April 2023 · Accepted: 7 July 2023 ·
Published Online: 24 July 2023

View Online
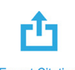
Export Citation

CrossMark

Hao Lu,[1,2,a)] Lei Li,[1] Zhiwu Tang,[1] Maji Xu,[1] Yonghui Zheng,[3] Martin Becker,[2] Yinmei Lu,[1] Mingkai Li,[1] Pai Li,[1] Zaoli Zhang,[3,a)] Peter J. Klar,[2] and Yunbin He[1,a)]

AFFILIATIONS

[1]Ministry-of-Education Key Laboratory of Green Preparation and Application for Functional Materials, Hubei Key Lab of Ferro & Piezoelectric Materials and Devices, Hubei Key Laboratory of Polymer Materials, and School of Materials Science & Engineering, Hubei University, Wuhan 430062, China
[2]Institute of Experimental Physics I and Center of Materials Research (ZfM/LaMa), Justus Liebig University Giessen, Giessen, Germany
[3]Erich Schmid Institute of Materials Science, Austrian Academy of Sciences, A-8700 Leoben, Austria

[a)]Authors to whom correspondence should be addressed: hao.lu@physik.uni-giessen.de; zaoli.zhang@oeaw.ac.at; and ybhe@hubu.edu.cn

ABSTRACT

We explore the possibility of tuning the metal-to-insulator transition (MIT) of crystalline VO_2 thin films by strain engineering. We deposit high-quality VO_2 epitaxial films of different thicknesses on TiO_2 (110) substrates by pulsed laser deposition. The strain state of the deposited film varies with its thickness. This allows us to correlate the MIT characteristics with the strain state of the VO_2 film by a careful characterization of the structural and electrical properties. Thin VO_2 films on TiO_2 (110) substrates are almost fully strained up to thicknesses of about 20 nm and exhibit tensile strain along the *c* axis of the (high-temperature) metallic rutile phase leading to an increase in the MIT temperature by as much as 30 °C in comparison to the almost fully relaxed 300 nm-thick VO_2 film. The strain gradient within the thicker samples leads to a continuous serial switching of layered regions of the VO_2 film from the insulating to the metallic state with increasing temperature.

© 2023 Author(s). All article content, except where otherwise noted, is licensed under a Creative Commons Attribution (CC BY) license (http://creativecommons.org/licenses/by/4.0/). https://doi.org/10.1063/5.0152809

In the vicinity of 68 °C, crystalline bulk vanadium dioxide (VO_2) undergoes a reversible structural phase transition from the high-temperature (HT) rutile phase to the low-temperature (LT) monoclinic phase which is accompanied by a metal-to-insulator transition (MIT).[1–3] When approaching the critical temperature T_C of the phase transition from below, the resistivity decreases by as much as five orders of magnitude at T_C,[4] and the optical transmittance in the near-infrared (NIR) region decreases significantly due to an increase in the reflectivity. Both effects are induced by the much increased free carriers in the metallic phase. Today, considerable effort is made to understand and manipulate the MIT in VO_2 thin films because such films serve as active functional materials in numerous device concepts, such as smart glass, storage media, and ultrafast switches.[5–7] There are many ways to tune the T_C of the MIT, such as doping and lattice strain.[8–11] In the case of high-quality epitaxial films, a variation of the MIT temperature can be achieved while keeping an abrupt phase transition in a narrow temperature window. Thus, a broad transition and a hysteresis of the switching between up- and down-sweep can be avoided. Such broadening often occurs when the transition temperature is tuned by doping.[12] Some studies address this issue by comparing the structural transition behavior of pure and doped VO_2 thin films grown on sapphire (Al_2O_3) substrates with the VO_2 bulk material.[13–15] An effective tuning of the transition temperature by strain is best achieved in the case of pseudomorphic growth of a crystalline thin film on a crystalline substrate of the same crystal structure and slightly different lattice constants. For example, rutile TiO_2 possesses the same crystal structure as the high-temperature VO_2 phase and comparable lattice parameters. Therefore, rutile TiO_2 substrates offer ideal conditions for the pseudomorphic growth of VO_2 thin films. Zhang *et al.* were the first to systematically study VO_2 films on TiO_2 substrates by transmission electron microscopy (TEM).[16] Basically, the MIT temperature of VO_2 varies with the spacing along the chain of V-atoms whose direction corresponds to the *a* and *c* axes of the monoclinic- and rutile-phase, respectively. Muraoka *et al.* reported that

27 September 2024 08:12:58

compressive strain along the c axis of very thin VO_2 films on rutile TiO_2 (100) and (110) substrates induced a reduction in the MIT temperature.[17] Zou *et al.* confirmed that the temperature of MIT in the interface region of epitaxial VO_2 films grown on rutile TiO_2 (001) using oxide molecular beam epitaxy depends on the strain state.[18] It should be noted that for VO_2 thin films pseudomorphically grown on crystalline TiO_2 substrates of various orientations different strain states can be induced. In the case of TiO_2 (001) substrates, the c axis is perpendicular to the substrate surface and the VO_2 layer is biaxially strained. In contrast, the c axis lies in the substrate plane when TiO_2 (110) substrates are used and the in-plane strains are not the same in the directions parallel and perpendicular to the c axis. As yet, a systematic analysis of the intrinsic relationship between lattice strain and MIT is lacking. However, a thorough understanding of the strain effects is essential for exploiting such a correlation in device concepts.

In this work, we prepared a series of VO_2 epitaxial films on rutile TiO_2 (110) substrates of various thicknesses by pulsed laser deposition (PLD) and studied the strain relaxation with increasing film thickness. VO_2 thin-film samples were deposited on rutile TiO_2 (110) substrates by PLD employing a KrF excimer laser (Lambda Physik COMPEX PRO 205 F, $\lambda = 248$ nm) as the ablation source. The laser beam energy was fixed at 600 mJ/pulse at a pulse repetition rate of 5 Hz. A VO_2 ceramic disk of high-purity (99.999%) was used as an ablation target. Additional O_2 gas was introduced into the chamber as reactive gas. The same growth conditions were used for all samples, only the number of pulses in the ablation process was varied to obtain different sample thicknesses. The O_2 pressure was kept at 1.0 Pa during the film growth. The TiO_2 (110) substrates were cleaned ultrasonically in acetone, ethanol, and de-ionized water, each for 15 min, and then transferred into the deposition chamber immediately after blow-dry with nitrogen gas. The target–substrate distance was set to 6 cm. The base pressure in the chamber was 1×10^{-4} Pa prior to letting in the O_2 reactive gas. The substrate temperature during the deposition was fixed at 600 °C. By varying the number of pulses in the ablation process from 500 to 18 000, we obtained a series of VO_2 films with thicknesses of 7 to 300 nm.

X-ray diffraction (XRD) and reciprocal space mapping (RSM) using a four-circle x-ray diffractometer (Bruker, D8 discover) with Cu $K\alpha$ radiation ($\lambda = 1.5406$ Å) were performed for the structural characterization of the deposited VO_2 films. The sample's electrical resistance in a linear configuration of four contacts is measured between 25 and 90 °C to investigate the electrical switching properties of the VO_2 films. Cross-sectional samples of the VO_2 thin films on rutile TiO_2 (110) substrates for TEM analyses were prepared in an FEI Helios 600 instrument with a standard lift-out and polishing process. After polishing, the samples were cleaned in a Gatan 691 PIPS at 0.8 keV to remove the residual contamination and possible damage. The high-angle annular dark-field (HAADF, $64 < \beta < 180$ mrad) images were recorded using the scanning-TEM mode of the JEM Grand ARM300F microscope with double spherical aberration (Cs) correctors.

Figure 1(a) depicts ω–2θ–XRD traces of VO_2 films of various thicknesses between 7 and 300 nm. The film thicknesses were determined by x-ray reflection for films with thicknesses below 100 nm, and for thicker films, the thickness was estimated using the growth rate per laser pulse established for the thinner samples (see Fig. S1 of the supplementary material). The lattice parameters of the rutile TiO_2 substrate ($a = b = 4.593$ and $c = 2.959$ Å) and of the rutile VO_2 ($a = b = 4.554$ and $c = 2.855$ Å) are very close.[19,20] In the case of pseudomorphic growth on a TiO_2 (110) substrate, the VO_2 films should experience an anisotropic in-plane strain (0.85% along the $[1–10]_r$

27 September 2024 08:12:58

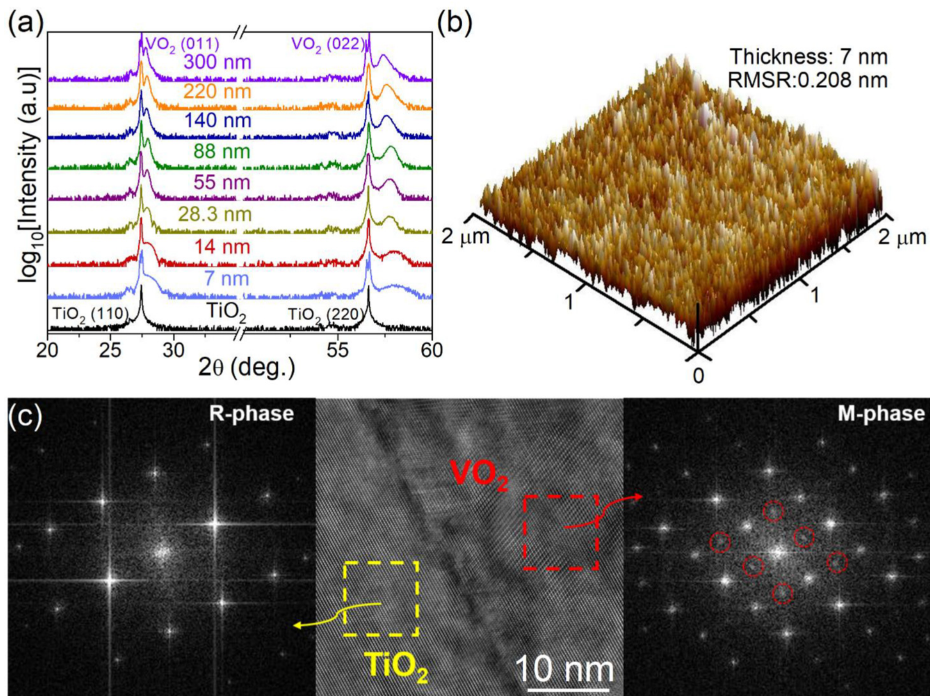

FIG. 1. (a) ω–2θ XRD traces of VO_2 films deposited on (110) TiO_2 substrates with various thicknesses. (b) AFM image of the surface of the 7 nm VO_2 film. (c) HRTEM image in the vicinity of the VO_2/TiO_2 interface of a sample with a 20 nm VO_2 film and corresponding FFT patterns.

© Author(s) 2023

direction and 3.5% along the $[001]_r$ direction) induced by the TiO_2 (110) substrates. The XRD traces show clear features of the VO_2 film in addition to the diffraction peaks from the TiO_2 (110) substrate. The two peaks close to 28° and 57° are assigned to diffraction from the monoclinic VO_2 $(011)_m$ and $(022)_m$ planes, respectively. No sign of polycrystalline or amorphous phases is present in the diffractogram, which demonstrates that a VO_2 film with domains of single orientation was prepared. Furthermore, we characterized the surface morphology of all grown VO_2 films by atomic force microscopy (AFM). Figure 1(b) shows an exemplary AFM image of the VO_2 film with a thickness of 7 nm. The surface of the film is dense and homogeneous, exhibiting small grains only. The root mean square roughness of all films averaged over a $2 \times 2\,\mu m^2$ surface area increases from 0.2 to 0.99 nm, when the film's thickness increases from 7 to 300 nm. Thus, all films grown can be considered smooth. Additional AFM images can be found in Fig. S2 of the supplementary material. The high-resolution TEM (HRTEM) data in Fig. 1(c) and the corresponding fast Fourier transformation (FFT) pattern confirm the assignment of the structures in the XRD analyses.

In Fig. 2(a), we zoom in into the region of ω–2θ XRD traces corresponding to the $(022)_m$ peak of monoclinic VO_2. The diffraction peak in the range from 58.05° to 57.44° depending on the VO_2 thickness is assigned to the monoclinic VO_2 $(022)_m$ plane, rather than the rutile $(220)_r$ plane. It is important to note for what follows that, according to this assignment, the *c* axis of the HT rutile phase of the VO_2 films deposited lies in the film plane. The ω–2θ XRD traces probe the lattice spacings of the VO_2 films in the growth direction, i.e., perpendicular to the *c* axis. In the case of pseudomorphic growth, the VO_2 film lattice is under tensile strain along the in-plane *c* axis of the HT rutile phase, as discussed above. Consequently, the lattice of the VO_2 film in the growth direction is expected to be compressively strained. As seen in Fig. 2(a), the $(022)_m$ diffraction peaks of the deposited VO_2 films of different thicknesses are located at various angles, which are all somewhat higher than that of the VO_2 bulk material (57.43° according to JCPDS No. 431051). This means that the $(022)_m$-plane interplanar spacings of all the deposited VO_2 films are shrunk relative to that of bulk VO_2. Thus, all the VO_2 films lattices are, indeed, under compressive strain as expected. With the increasing film thickness from 7 to 300 nm, the VO_2 $(022)_m$ diffraction peak gradually shifts to lower angles, indicating a continuous increase in the $(022)_m$ interplanar spacing and hence gradual relaxation of the compressed monoclinic VO_2 $(022)_m$ lattice along the film growth direction. The very thin VO_2 films of 7 and 14 nm thicknesses show an almost identical (022)m diffraction angle of 58.05° and can be regarded as fully strained to fit the TiO_2 (110) substrate. The strain energy builds up with increasing film thickness. At a critical film thickness of about 20 nm, the deposited VO_2 films start to relax, and their (022)m interplanar spacings approach continuously that of unstrained VO_2 bulk material. Almost complete relaxation has occurred at the film thickness of 300 nm. However, the $(022)_m$ diffraction peak of the 300 nm-thick VO_2 film is not symmetric, showing a pronounced tail on its right. This asymmetry of the diffraction peak reflects the strain distribution within the film, i.e., the strain state of the film gradually varies from the substrate–film interface toward the film surface. Thus, in thicker VO_2 films, this transition of the strain state can be roughly approximated by three regions with different strain states: fully strained (almost pseudomorphic growth), partially relaxed, and (almost) fully relaxed [corresponding positions of the $(022)_m$ diffraction peaks are indicated by red lines in Figs. 2(a) and 2(b)].

Figure 2(b) shows the results of RSM taken at 30 °C, i.e., below T_C where the VO_2 films are still in their LT monoclinic phase. The diffraction spots corresponding to the (220) planes of the rutile TiO_2

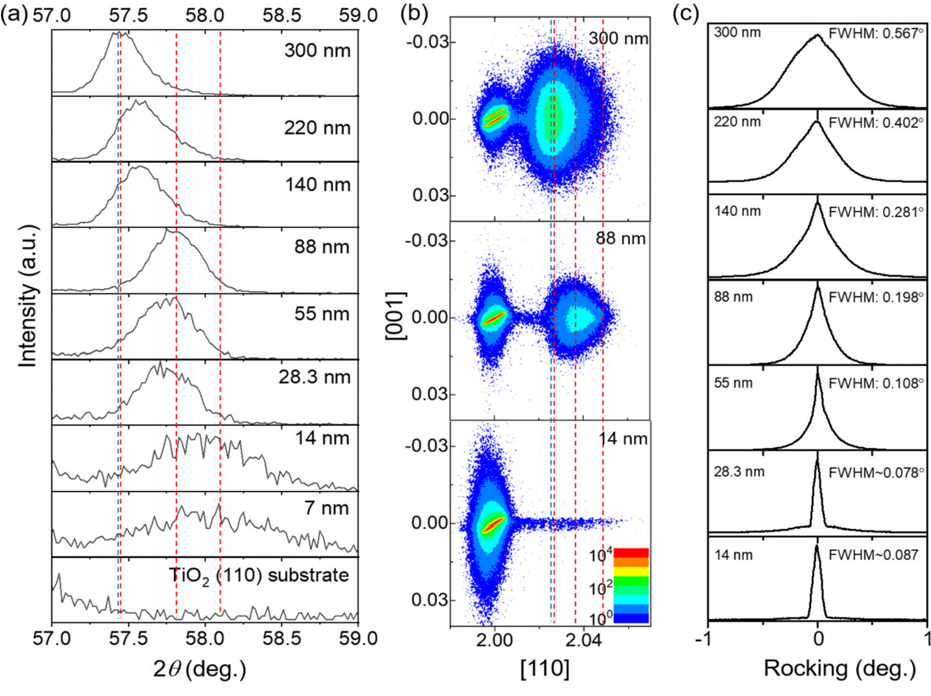

FIG. 2. (a) Zoom in ω–2θ XRD patterns of VO_2 films. (b) RSM images in the vicinity of the $(022)_m$ diffraction peak of the VO_2 films. (c) Rocking curves of the VO_2 $(011)_m$ plane of all films. All data were recorded at 30 °C.

27 September 2024 08:12:58

© Author(s) 2023

substrate are visible on the left-hand side of the maps, and the diffraction spots of VO_2 $(022)_m$ planes occur on the right-hand side. The position of VO_2 $(022)_m$ diffraction spot gradually shifts toward to that of bulk VO_2 with the increasing film thickness from 14 via 88 to 300 nm, reflecting that the average strain in the film decreases with the increasing film thickness. The RSM results corroborate the $(022)_m$ peak shift trend of the ω–2θ XRD traces. In addition, we performed rocking-curve XRD measurements of $(011)_m$ planes to evaluate the out-of-plane atomic ordering of the deposited single-crystalline VO_2 films. The relation between the full width at half maximum (FWHM) of the XRD ω-scan rocking curves and the thickness of the VO_2 thin films is shown in Fig. 2(c). The FWHM increases from 0.078° to 0.567° when the film thickness increases from 28.3 to 300 nm. The increasing inhomogeneity and atomic disorder of the film can as well be interpreted in terms of the strain relaxation, which progresses with the increase in thickness.

Different strain states of the VO_2 lattice affect the phase transition temperature T_C of the MIT. The determination of T_C is not straightforward, in particular, when the transition takes place in a broader temperature window due to inhomogeneity of the VO_2 sample, e.g., in our case, due to a strain distribution along the growth direction of the VO_2 film. There are different ways of defining and determining a value for T_C in such cases, which lead to slightly different values, but reveal similar trends. Here, we focus on the change in the film resistivity ρ with temperature and determine T_C by the average of the positions of the minima of plots $d(\log\rho)/dT$ vs T measured during heating and cooling of the sample. Corresponding plots of resistivity ρ and $d(\log\rho)/dT$ vs T are shown in Figs. 3(a) and 3(b), respectively, for the samples with thicknesses of 7, 88, and 300 nm. The $d(\log\rho)/dT$ curves of all VO_2 films studied are shown in Fig. S3 of the supplementary material.

The thinnest VO_2 film with a thickness of 7 nm exhibits the highest T_C of 75.6 °C, which is anticipated from the XRD analysis as it possesses the longest c lattice parameter in the rutile phase due to the tensile strain in-plane of the film. Although strain relaxation sets in already at a film thickness of 14 nm, which leads to a slightly lowered T_C (74.8 °C). Drastic T_C drop occurs at the film thicknesses between 14 and 28.3 nm. T_C is already lowered down to about 55 °C at a thickness of 88 nm and further down to 49.4 °C for the 300 nm thick film. It is worth noting that the T_C values determined for the 88 and 300 nm VO_2 films are in concordance with the values revealed by RSM (see Fig. 4 for the 88 and 300 nm samples). Nevertheless, it is somewhat surprising that the T_C values of almost relaxed samples are lower than the T_C of bulk VO_2. As both methods yield similar results, we believe that the determined T_C values are reliable and this finding is due to non-stoichiometry, i.e., occurrence of oxygen vacancies in the deposited films, as reported by other researchers,[21,22] and confirmed by our x-ray photoelectron spectroscopy (XPS) measurements presented in Figs. S4 and S5. Nevertheless, Raman measurements in Fig. S6 of the supplementary material show that the deposited films are of M1-phase VO_2 despite the non-stoichiometry. Furthermore, the $d(\log \rho)/dT$ vs T curve exhibits an asymmetry for larger film thicknesses. A wing develops on the HT side of the minimum. This asymmetric minimum with the extended HT wing is clearly visible in the case of 88 nm film thickness and more pronounced in the 140 nm thick film (see Fig. S3 of the supplementary material) and further turns into a pronounced shoulder with virtually another minimum in the case of the thickest sample grown, i.e., the 300 nm VO_2 film. Thus, the shape of the $d(\log \rho)/dT$ curve reflects the strain distribution from the substrate-film interface to the film surface. The local strain state determines the local transition temperature inside the film. The layers parallel to the interface exhibit the same strain state, and the transition temperature decreases with increasing distance from the interface. Therefore, the metallic state across the entire film of the inhomogeneously strained samples is anticipated to be gradually established with the increasing temperature. It initializes in the vicinity of the film surface and finally reaches the layers close to the film–substrate interface. The samples with thicknesses in the range of 50–200 nm show the largest inhomogeneity due to strain. This is also reflected in Fig. 3(c), where the variation of $T_C = (T_{C,Heating} + T_{C,Cooling})/2$ with film thickness is plotted together with the thermal hysteresis width $\Delta T = T_{C,Heating} - T_{C,Cooling}$, in which $T_{C,Heating}$ and $T_{C,Cooling}$ are the transition temperatures determined at the minima of the $d(\log \rho)/dT$ curves corresponding to heating and cooling processes, respectively. Figure 3(d) illustrates schematically the three regions, namely, pseudomorphically/fully strained, partially relaxed, and fully relaxed, in the deposited VO_2 film as we proposed based on the above-mentioned discussions.

The *in situ* temperature-dependent high-resolution XRD-RSM results provide more evidence for the gradual structural phase

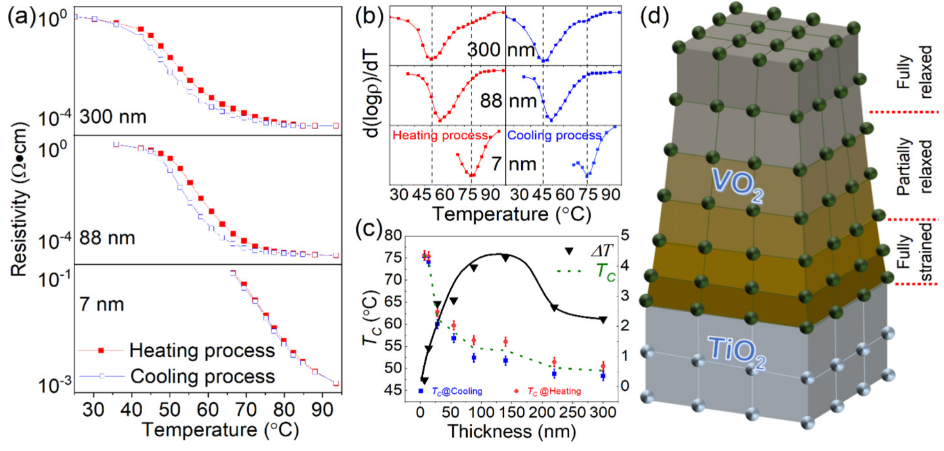

FIG. 3. (a) Temperature dependence of electrical resistivity. (b) Derivative curves (d[log (ρ)]/dT) as a function of temperature. (c) MIT transition temperature T_C and thermal hysteresis width ΔT as a function of film thicknesses. (d) Schematic illustration of the strain relaxation in a thick VO_2 thin film.

27 September 2024 08:12:58

© Author(s) 2023

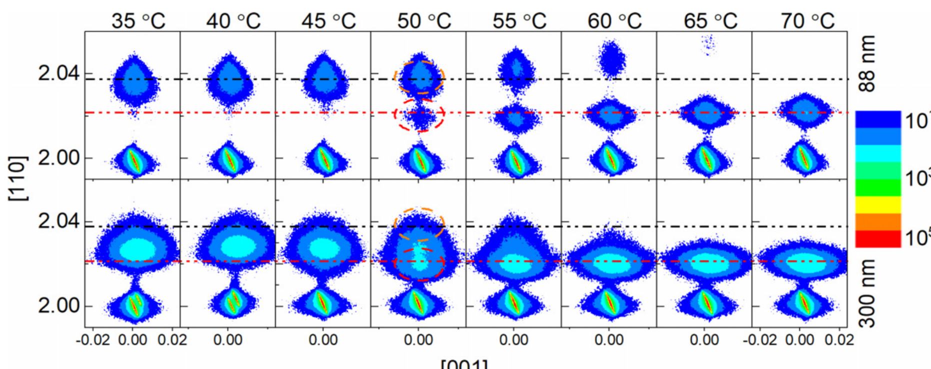

FIG. 4. RSM images of 88 and 300 nm thick VO_2 films on a rutile TiO_2 (110) substrate in the vicinity of the $(022)_m$ diffraction peak of monoclinic VO_2 as a function of temperature. The abscissae scales remain consistent, and to prevent the overlap of abscissa values in each image, only the complete values of the *x* axis for the panels on the far left and far right are displayed.

transition of the VO_2 films. Figure 4 shows RS maps obtained at various temperatures between 35 and 70 °C from the 88 and 300 nm thick VO_2 films with T_C of about 55 and 49.4 °C. The maps were recorded in the vicinity of the diffraction peak corresponding to $(022)_m$ planes of VO_2. The change in the central position of diffraction spots in reciprocal space mapping reflects the phase transition. Up to three diffraction spots can be discerned in maps associated with the phase transition. The bottom diffraction spot in the map corresponds to the (220) diffraction of the rutile TiO_2 substrate. The other two, one at the top and another in the middle of the map, disappears and appears, respectively, with increasing temperature. The top diffraction spot, which gradually fades away with increasing temperature, corresponds to the diffraction of $(022)_m$ planes of VO_2 in the LT monoclinic phase. The intermediate diffraction spot, which gradually appears with increasing temperature, arises from $(220)_r$ diffraction of VO_2 in the HT rutile phase. The position and intensity variation of diffraction spots of the 88 nm thick VO_2 film unanimously show that the phase transition gradually takes place in a rather broad temperature range between 50 and 65 °C. In this temperature range, both phases of VO_2, the metallic rutile phase and the insulating monoclinic phase, are present simultaneously in accordance with the interpretation of the temperature-dependent electrical measurements. At about 50 °C, metallic rutile-phase regions of the VO_2 film start to appear nearly the surface and at about 65 °C the last insulating monoclinic-phase regions close to the film–substrate interface lose their insulating character and become metallic. Between 30 and 45 °C, the VO_2 is solely in the insulating monoclinic-phase. Above 65 °C, the diffraction spot from the monoclinic (022) plane has disappeared, and the entire VO_2 film is transformed into the rutile phase. The phase transition exhibited by the 300 nm VO_2 film follows a comparable pattern. However, when comparing in detail the RSMs of both films at the same temperature in the vicinity of T_C, such as 50 °C, evident differences appear. For the 88 nm-thick film, the diffraction spot associated with the rutile structure is somewhat weaker in intensity than that corresponding to the monoclinic structure. Conversely, in the 300 nm film, the diffraction spot related to the rutile structure appears stronger than that associated with the monoclinic structure. This observation suggests that at 50 °C a greater number of regions are strain relaxed within the thicker film. These regions contribute to a lower overall phase transition temperature compared to the thinner film of 88 nm. The structural evolution deduced from RSMs recorded at different temperatures supports our proposal that the strain relaxation in VO_2 thin films grown on TiO_2 (110) substrates causes the reduction in the phase transition temperature of the film.

In summary, we provide further evidence that the phase transition temperature and the width of the temperature range where the MIT transition in VO_2 takes place depend on the strain distribution in the crystalline VO_2 layers. The strain distribution, in turn, depends on the choice of substrate, its orientation, and the thickness of the deposited VO_2 film. In particular, we demonstrate that the transition temperature in the case of crystalline VO_2 films deposited on TiO_2 (110) substrates can be varied by about 30 °C from above to below the T_C of bulk VO_2 when increasing the thickness of the deposited VO_2 film from 7 (almost fully strained) to 300 nm (almost fully relaxed). The strain gradient along the growth direction leads to a continuous serial switching of layer-like regions of the film into the metallic state with increasing temperature. The serial switching starts from the almost fully relaxed region near the surface and ends at the almost entirely strained region at the substrate–film interface.

See the supplementary material for XRR spectra, AFM images, and temperature-dependent electrical resistivity and derivative ($d[\log(\rho)]/dT$) curves recorded during film heating and cooling for VO_2 films of various thicknesses; XPS survey and high-resolution spectra acquired for the 28.3 and 140 nm-thick films and Raman spectra of the 140 nm-thick VO_2 film and the TiO_2 substrate; and a table of FWHM, MIT temperature, RMSR, and the lattice parameters calculated from RSM measurements for VO_2 films of different thicknesses.

This work was supported by the National Natural Science Foundation of China (Grant Nos. 51572073, 11975093, and 62274057), the Sino-German Mobility Program (Grant No. M-0764), the Natural Science Foundation of Hubei Province (Grant Nos. 2019CFA006, 2021EHB005, and 2022EHB023), the Program for Science and Technology Innovation Team in Colleges of Hubei Province (Grant No. T201901), and the China Scholarship Council (award to Hao Lu for 3 year's study abroad at the University of Giessen). Furthermore, we acknowledge the support from the German BMBF (Grant No. 03VP09691), the Austrian innovation fund (with Project No. ÖAW 4023 Innovation funds), and DFG research grant 510965362.

AUTHOR DECLARATIONS

Conflict of Interest

The authors have no conflicts to disclose.

27 September 2024 08:12:58

© Author(s) 2023

Author Contributions

Hao Lu: Conceptualization (equal); Data curation (equal); Formal analysis (equal); Investigation (equal); Methodology (equal); Writing – original draft (lead); Writing – review & editing (lead). **Zaoli Zhang:** Funding acquisition (equal); Writing – review & editing (equal). **Peter J. Klar:** Formal analysis (lead); Funding acquisition (lead); Supervision (lead); Writing – original draft (equal); Writing – review & editing (lead). **Yunbin He:** Formal analysis (lead); Funding acquisition (lead); Supervision (lead); Writing – original draft (equal); Writing – review & editing (lead). **Lei Li:** Conceptualization (equal); Data curation (equal); Methodology (equal); Writing – original draft (equal). **Zhiwu Tang:** Data curation (equal); Methodology (equal). **Maji Xu:** Data curation (equal); Methodology (equal). **Yonghui Zheng:** Data curation (equal); Formal analysis (equal). **Martin Becker:** Formal analysis (equal); Investigation (equal); Writing – review & editing (equal). **Yinmei Lu:** Conceptualization (equal); Funding acquisition (equal). **Mingkai Li:** Conceptualization (equal); Funding acquisition (equal). **Pai Li:** Funding acquisition (equal).

DATA AVAILABILITY

The data that support the findings of this study are available within the article and its supplementary material.

REFERENCES

[1]F. J. Morin, "Oxides which show a metal-to-insulator transition at the Neel temperature," Phys. Rev. Lett. **3**(1), 34 (1959).

[2]J. B. Goodenough, "The two components of the crystallographic transition in VO_2," J. Solid State Chem. **3**(4), 490–500 (1971).

[3]J. Narayan and V. M. Bhosle, "Phase transition and critical issues in structure-property correlations of vanadium oxide," J. Appl. Phys. **100**(10), 103524 (2006).

[4]H. S. Choi, J. S. Ahn, J. H. Jung, T. W. Noh, and D. H. Kim, "Mid-infrared properties of a VO_2 film near the metal-insulator transition," Phys. Rev. B **54**(7), 4621 (1996).

[5]F. Kuhl, M. Becker, S. L. Benz, J. Hauptmann, J. Kessler, S. Chatterjee, A. Polity, and P. J. Klar, "Embedding quaternary $V_{1-x-y}Sr_xW_yO_2$ into multilayer systems to enhance its thermochromic properties for smart glass applications," ACS Appl. Electron. Mater. **4**(1), 513–520 (2022).

[6]A. W. Smith, "Optical storage in VO_2 films," Appl. Phys. Lett **23**(8), 437–438 (1973).

[7]M. F. Becker, A. B. Buckman, R. M. Walser, T. Lépine, P. Georges, and A. Brun, "Femtosecond laser excitation of the semiconductor-metal phase transition in VO_2," Appl. Phys. Lett. **65**(12), 1507–1509 (1994).

[8]H. Lu, L. Chen, R. Cao, X. Tao, X. Wang, M. Li, P. Li, Y. Lu, P. J. Klar, and Y. He, "$RuVO_2$ alloy epitaxial films: Lowered insulator–metal transition temperature and retained modulation capacity," Appl. Phys. Lett **116**(19), 192103 (2020).

[9]J. Jian, X. Wang, L. Li, M. Fan, W. Zhang, J. Huang, Z. Qi, and H. Wang, "Continuous tuning of phase transition temperature in VO_2 thin films on c-cut sapphire substrates via strain variation," ACS Appl. Mater. Interfaces **9**(6), 5319–5327 (2017).

[10]H. Li, J. Wang, Z. You, Y. Yu, P. Li, L. Xiong, and Y. He, "Nb-doped VO_2 thin films with enhanced thermal sensing performance for uncooled infrared detection," Mater. Res. Bull. **146**, 111615 (2022).

[11]H. Guo, K. Chen, Y. Oh, K. Wang, C. Dejoie, S. A. Syed Asif, O. L. Warren, Z. W. Shan, J. Wu, and A. M. Minor, "Mechanics and dynamics of the strain-induced M1–M2 structural phase transition in individual VO_2 nanowires," Nano Lett. **11**(8), 3207–3213 (2011).

[12]X. Wang, L. Chen, H. Lu, W. Fang, H. Li, W. Yin, M. Li, Y. Lu, P. Li, and Y. He, "Enhancing visible-light transmittance while reducing phase transition temperature of VO_2 by Hf–W co-doping," Appl. Phys. Lett. **118**, 192102 (2021).

[13]P. Jin, M. Tazawa, K. Yoshimura, K. Igarashi, S. Tanemura, K. Macak, and U. Helmersson, "Epitaxial growth of W-doped VO_2/V_2O_3 multilayer on α-Al_2O_3 (110) by reactive magnetron sputtering," Thin Solid Films **375**(1–2), 128–131 (2000).

[14]J. M. Gregg and R. M. Bowman, "The effect applied strain resistance VO2 thin films," Appl. Phys. Lett. **71**(25), 3649–3651 (1997).

[15]V. Théry, A. Boulle, A. Crunteanu, J. C. Orlianges, A. Beaumont, R. Mayet, A. Mennai, F. Cosset, A. Bessaudou, and M. Fabert, "Role of thermal strain in the metal-insulator and structural phase transition of epitaxial VO_2 films," Phys. Rev. B **93**(18), 184106 (2016).

[16]Y. Zheng, Z. Chen, H. Lu, Y. Cheng, X. Chen, Y. He, and Z. Zhang, "The formation of TiO_2/VO_2 multilayer structure via directional cationic diffusion," Nanoscale **13**(16), 7783–7791 (2021).

[17]Y. Muraoka and Z. Hiroi, "Metal–insulator transition of VO_2 thin films grown on TiO_2 (001) and (110) substrates," Appl. Phys. Lett. **80**(4), 583–585 (2002).

[18]L. L. Fan, S. Chen, Z. L. Luo, Q. H. Liu, Y. F. Wu, L. Song, D. X. Ji, P. Wang, W. S. Chu, C. Gao, and C. W. Zou, "Strain dynamics of ultrathin VO_2 film grown on TiO_2 (001) and the associated phase transition modulation," Nano Lett. **14**(7), 4036–4043 (2014).

[19]H. E. Swanson, *Standard X-Ray Diffraction Powder Patterns* (U.S. Department of Commerce, National Bureau of Standards, 1953).

[20]K. D. Rogers, "An X-ray diffraction study of semiconductor and metallic vanadium dioxide," Powder Diffr. **8**(4), 240–244 (1993).

[21]S. Fan, L. Fan, Q. Li, J. Liu, and B. Ye, "The identification of defect structures for oxygen pressure dependent VO_2 crystal films," Appl. Surf. Sci. **321**, 464–468 (2014).

[22]Q. Lu, C. Sohn, G. Hu, X. Gao, M. F. Chisholm, I. Kylänpää, J. T. Krogel, P. R. Kent, O. Heinonen, P. Ganesh, and H. N. Lee, "Metal–insulator transition tuned by oxygen vacancy migration across TiO_2/VO_2 interface," Sci. Rep. **10**(1), 18554 (2020).

27 September 2024 08:12:58

© Author(s) 2023